European Polymer Journal 220 (2024) 113473

Contents lists available at ScienceDirect

European Polymer Journal

journal homepage: www.elsevier.com/locate/europolj

Probing the inner structure and dynamics of pH-sensitive block copolymer nanoparticles with nitroxide radicals using scattering and EPR techniques

Svetlana Lukáš Petrova [a,*], Alessandro Jäger [a], Ewa Pavlova [a], Martina Vragović [a], Eliézer Jäger [a], Miloš Steinhart [a], Damir Klepac [b,c,*]

[a] Institute of Macromolecular Chemistry, Czech Academy of Sciences, Heyrovskeho nam. 2, Prague 6 162 06, Czech Republic
[b] Faculty of Medicine, University of Rijeka, Braće Branchetta 20, Rijeka HR-51000, Croatia
[c] Centre for Micro- and Nanosciences and Technologies, University of Rijeka, Radmile Matejčić 2, Rijeka HR-51000, Croatia

ARTICLE INFO

Keywords:
pH-responsive diblock copolymers
Nitroxide radicals
EPR
Microfluidic nanoprecipitation
Core–shell nanoparticles

ABSTRACT

This research emphasizes the crucial role of electron paramagnetic resonance (EPR) spectroscopy in nanoparticle analysis, showcasing its distinctive ability to probe molecular-level details. We demonstrate the synthesis and self-assembly of a new class of pH-responsive amphiphilic diblock copolymers, specifically poly[*N*-(2-hydroxypropyl)-methacrylamide]-*block*-poly[2-(diisopropylamino)ethyl methacrylate] (PHPMA-*b*-PDPA), incorporating 2,2,6,6-tetramethylpiperidine-1-oxyl (TEMPO) radicals covalently bound to the hydrophilic PHPMA segment. The copolymer synthesis involved a three-step process, combining reversible addition – fragmentation chain transfer (RAFT) polymerization with carbodiimide (DCC) chemistry. TEMPO radical-containing nanoparticles (RNPs) were created using microfluidic (MF) nanoprecipitation, a technique essential for generating uniform nanoparticles with predictable biodistribution and cellular uptake. Adjusting MF protocol parameters allowed fine-tuning of RNP sizes. EPR spectroscopy confirmed the formation of core–shell RNPs, with features aligning closely with those obtained from scattering techniques like dynamic light scattering (DLS), static light scattering (SLS), small-angle X-ray scattering (SAXS), and cryo-transmission electron microscopy (cryo-TEM). EPR spectroscopy emerges as a potent tool for molecular-level analysis of colloidal polymer systems. This study highlights the EPR-spin label method's efficacy in probing the internal structural features and dynamics of core–shell nanoparticles, especially their response to pH-triggered disassembly. The findings open new avenues for the use of pH-responsive TEMPO-labeled diblock copolymers in controlled drug delivery applications.

1. Introduction

In the last ten years, substantial advancements have been achieved in creating stimuli-responsive, or "smart" polymers. These polymers are sensitive to specific external triggers, such as temperature [1,2], light, electrical or magnetic fields [3], and chemicals. Researchers have investigated multiple facets of stimuli-responsiveness, such as the synthesis of responsive monomers, their polymerization processes, and the development of higher-order organized structures. This rapidly expanding field has been the subject of many comprehensive reviews [4–8]. Stimuli-responsive polymer nanoparticles (NPs) hold great protentional for applications in drug delivery and diagnostics due to their easy design, excellent biocompatibility, diverse structural options, and biomimetic properties. The structural characteristics of the NPs, influenced by factors such as molecular weight, hydrophobic to hydrophilic ratio, and preparation method, play a crucial role in modulating drug release kinetics and ensuring optimal therapeutic outcomes. Although straightforward methodologies have been thoroughly researched with notable success, particularly in controlling particle size and enhancing encapsulation efficiency by adjusting nanoprecipitation conditions, further investigation is required to minimize the polydispersity of self-assembled nanostructures. Utilizing microfluidic devices for this objective is a crucial strategy [9,10]. The microfluidic technique offers a powerful and versatile platform for the precise synthesis of NPs, with significant advantages in terms of control, efficiency, and scalability [11,12].

It is noteworthy that, in addition to core–shell NPssuch as polymer micelles and vesicles obtained from the solution self-assembly of block copolymers (BCs), there are also two-dimensional (2D) core–shell NPs [13–15]. These 2D systems have garnered increasing interest due to

* Corresponding authors.
E-mail addresses: petrova@imc.cas.cz (S. Lukáš Petrova), damir.klepac@medri.uniri.hr (D. Klepac).

https://doi.org/10.1016/j.eurpolymj.2024.113473
Received 16 July 2024; Received in revised form 10 September 2024; Accepted 22 September 2024
Available online 23 September 2024

their broad applications in materials science. Recently, Tong's group demonstrated the preparation of 2D, size-tunable, water-dispersible micelles with tailored compositions for pH-responsive drug release systems [16].

A particularly promising candidate in this field of the "smart" polymers is the pH-responsive polymer poly[2-(diisopropylamino)ethyl methacrylate], (PDPA) [17] due to its pKa of approximately 6.8 and its ability to dissociate rapidly at pH levels below 6.8 [18,19]. This is especially significant because endocytosis occurs swiftly, with the entire process, from plasma membrane wrapping to reaching the lysosomal stage, taking approximately 30 min [20]. PDPA-based NPs have demonstrated potential in precisely controlling drug release within specific pH ranges, accommodating both hydrophobic and hydrophilic drugs [21,22]. On the other hand, the utilization of biocompatible hydrophilic blocks, such as poly(*N*-(2-hydroxypropyl)methacrylamide) (PHPMA) in designing NPs has garnered significant attention in pharmaceutical technology [23]. The appeal of PHPMA for biomedical applications stems from its distinct attributes, including hydrophilicity, non-toxicity, and non-immunogenicity [24–26] making it the most promising alternative to polyethylene glycol-based materials [27]. In our previous study [28], we successfully synthesized a well-defined class of amphiphilic poly(ε-caprolactone)-*b*-poly(*N*-(2-hydroxypropyl)methacrylamide), PCL-*b*-PHPMA diblock copolymers, which are both biocompatible and biodegradable, and incorporated nitroxyl radicals into them. Subsequently, we evaluated the formation of micelles in aqueous media. To gain insights into the dynamic processes involved in self-assembly, we utilized electron paramagnetic resonance (EPR) spectroscopy. EPR spectroscopy has emerged as a valuable technique for studying polymers, offering insights into their structure and dynamics [29]. By introducing stable "spin labels" such as the 2,2,6,6-tetramethylpiperidine-1-oxyl (TEMPO) nitroxide radical into the target macromolecule, EPR analysis can provide valuable information on its internal structural characteristics [30,31]. Moreover, such radical containing polymers and nanoparticles (RNPs) have shown considerable potential for various applications. Yoshitomi *et al.* have designed a polymer with covalently linked nitroxide radicals that can be applied for scavenging reactive oxygen species from cigarette smoke [32]. pH-responsive RNPs composed of poly(chloromethylstyrene) (PCMS) and poly(ethylene glycol) (PEG) have shown therapeutic effect in the treatment of cerebral ischemia – reperfusion injury [33]. Another RNPs based on poly (ethylene glycol) (PEG) and poly[4-(2,2,6,6-tetramethylpiperidine-1-oxyl)aminomethylstyrene] have been found to reduce the tumorigenic characteristics of the triple negative breast cancer both *in vitro* and *in vivo* without side effects [34,35]. Such redox nanoparticles have also been investigated as possible nanotherapeutics in the treatment of colon cancer associated with colitis. In response to oral administration, RNP preferentially accumulated in cancer tissues, leading to a substantial reduction in tumor growth [36].

Doxorubicin (DOX) loaded pH-responsive NPs based on PHPMA-*b*-PDPA diblock copolymers have been studied previously [37]. When compared to free DOX, the drug-loaded NPs significantly improved therapeutic efficacy by inhibiting the growth of lymphoma tumors in the EL4 lymphoma model with reduced cardiotoxic effects [38]. In addition, it was found that these NPs are considerably more permeable than ROS-(reactive oxygen species) responsive or nonresponsive analogues and DOX is rapidly released in acidic medium following the NP disassembly [39].

This study introduces a novel approach, marking the first report of the synthesis and microfluidic-controlled self-assembly of pH-responsive amphiphilic PHPMA-*b*-PDPA diblock copolymers with spin-labeled functionality. In a three-step synthetic process, 4-amino-TEMPO radicals were covalently attached to the hydrophilic segment of the copolymer by combining reversible addition–fragmentation chain transfer (RAFT) polymerization with carbodiimide chemistry (DCC method). Spherical nanoparticles labeled with TEMPO radicals were successfully produced under physiological buffer conditions (phosphate-buffered saline, PBS, pH 7.4) using microfluidic (MF) nanoprecipitation. To provide unique revelations into the dynamic processes during the self-assembly of these labeled nanoparticles, we employed a combination of EPR spectroscopy with dynamic light scattering (DLS), static light scattering (SLS), small-angle X-ray scattering (SAXS), and cryo-transmission electron microscopy (cryo-TEM). This comprehensive characterization allowed us to assess the internal structure and physicochemical properties of the core–shell nanoparticles in exceptional detail. Notably, EPR spectral analysis revealed a unique correlation between the EPR line shape and the core–shell size and density measured by scattering techniques, offering new insights into nanoparticle behavior. Additionally, we investigated the pH-induced disassembly of the nanoparticles using EPR, demonstrating the versatility and broad potential of this method. By establishing novel correlations between nanoparticle structural characteristics, copolymer properties, and preparation methods, this research significantly advances the understanding and application of stimuli-responsive polymer nanoparticles in drug delivery and related fields (Fig. 1).

2. Materials and methods

2.1. Materials

The monomer *N*-(2-hydroxypropyl)methacrylamide (HPMA) (Scheme S1) was synthesized following the procedure outlined in reference [40]. The RAFT agent 4-cyano-4-(((ethylthio)carbonothioyl) thio)pentanoic acid (CTA) (Fig. S2) was synthesized following the method described in reference [41]. The complete synthesis procedures are detailed in the ESI file. The monomer 2-(diisopropylamino)ethyl methacrylate (DPA, purity ~ 97 %) was distilled under an argon atmosphere. 4,4′-Azobis(4-cyanovaleric acid) (V-501, ≥98 %) *N*,*N*′-dicyclohexylcarbodiimide (DCC, purity ~ 99 %) and 4-amino-2,2,6,6-tetramethylpiperidine-1-oxyl (4-amino-TEMPO, purity > 97 %). *N*,*N*-Dimethylformamide (DMF, ≥99.5 %, Sigma-Aldrich) was dried over CaH_2 and distilled under reduced pressure. Other solvents included diethyl ether (Et_2O, ≥ 99.7 %), and *tert*-butanol (*tert*-BuOH, ≥ 99.5 %) were used without further purification. All reagents and solvents were purchased from Sigma-Aldrich.

2.2. Characterization techniques

Detailed explanations of the employed characterization techniques are comprehensively presented in the Supplementary Information (ESI) file.

2.3. RAFT polymerization of HPMA using MWI (Scheme 1, (1))

The RAFT experiment was conducted in a 20 mL Biotage high-precision MW glass vial using a Biotage Initiator Robot Sixty laboratory MW reactor under normal voltage conditions, with a preliminary stirring step of 60 s. The standard RAFT polymerization procedure involved dissolving HPMA (1.0 g, 2.2×10^{-4} mol, degree of polymerization 35), CTA (57.62 mg, 2.2×10^{-4} mol), and initiator V-501 (30.83. mg, 0.11×10^{-4} mol) (with a [CTA]/[I] ratio of 1/0.2) in 5.0 mL of *tert*-BuOH. The solution was placed in a glass vial equipped with a magnetic

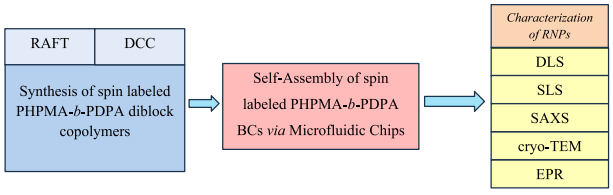

Fig. 1. A general diagram illustrating the relationship between the multi-step synthesis process and the techniques applied in this study.

stir bar, sealed, and purged with argon for 30 min to remove oxygen. The vial was then positioned in the MW instrument set at 75 °C for 3 h. Polymerization was terminated by stopping the MW irradiation, removing the vial from the instrument, and rapidly cooling it in liquid nitrogen. A 25 μL aliquot was immediately analyzed by ^{1}H NMR spectroscopy to determine monomer conversion by comparing the remaining monomer concentration to the initial feed. The polymerization solution was precipitated with cold acetone or a mixture of acetone / diethyl ether (3/1, v/v), followed by centrifugation to isolate the product. The isolated PHPMA macroCTA was dissolved in a small methanol and purified using Sephadex LH-20 chromatography with methanol as the mobile phase. The product was then precipitated in cold diethyl ether and vacuum-dried to obtain a yellow solid. The resulting homopolymer was characterized by size exclusion chromatography (SEC) and ^{1}H NMR spectroscopy (refer to Table 1 for details).

2.4. Synthesis of PHPMA-b-PDPA diblock copolymers (Scheme 1(2))

The RAFT polymerization was conducted using different molar ratios of monomers to achieve PDPA blocks with varying molecular weights: [DPA]/[CTA]/[I] = 30/1/0.2 and [DPA]/[CTA]/[I] = 97/1/0.2, respectively. In a Schlenk flask equipped with a magnetic stirrer, PHPMA macroCTA agent (80.0 mg, 1.52×10^{-5} mol) was dissolved in methanol (2.0 mL). Separately, varying amounts of the monomer DPA (62.41 μL for DP 30 and 187 μL for DP 90) were dissolved in 2.5 mL of 1,4-dioxane. The solutions were then combined, and 0.5 mg of the initiator AIBN (3.04×10^{-5} mol), dissolved in 100 μL of DMSO, was added under continuous stirring. The polymer mixture was purged with argon for 30 min and then placed in an oil bath preheated to 75 °C for approximately 16 h. Polymerization was terminated by rapid cooling, freezing, and exposure to air for quenching. The block copolymers were purified by dialyzing against deionized water at a pH of ~ 3 for 48 h, using a membrane with a molecular weight cut-off (MWCO) of 3.5 kDa, with the water being changed every 12 h. The block copolymers were then recovered by lyophilization and characterized using ^{1}H NMR and SEC.

2.5. Spin labeling of PHPMA-b-PDPA BCs (Scheme 1(3))

The TEMPO-labeled pH-responsive PHPMA-*b*-PDPA BCs were synthesized via the carbodiimide (DCC) method. The spin-labeled BCs were prepared with variations in the mole ratios of PHPMA-*b*-PDPA and 4-amino-TEMPO reactants. In a 25 mL flame-dried, argon-purged two-neck round-bottom flask equipped with three-port valves, 0.1 g (9.1×10^{-6} mol) of PHPMA-*b*-PDPA diblock copolymer was dissolved in dry DMF (5.0 mL). Separately, DCC (11.3 mg, 5.46×10^{-5} mol, 6.0 eq excess) was dissolved in dry DMF (0.5 mL), and 4-amino-TEMPO (69.5 mg, 5.46×10^{-5} mol, 6.0 eq excess,) was dissolved in another 0.5 mL of dry DMF. Both solutions were then carefully transferred to the flask under an inert gas atmosphere and stirred at room temperature for 72 h under argon. The spin-labeled block copolymers were then purified by dialysis against deionized water at a pH of ~ 3 for 48 h, using a membrane with a molecular weight cut-off (MWCO) of 3.5 kDa, with water changes every 12 h. The block copolymers were recovered by lyophilization and characterized using SEC.

Table 1
Experimental conditions and macromolecular characteristics of the PHPMA-mCTA and pH-responsive $PHPMA_{32}$-*b*-$PDPA_m$ BCs.

Sample	$[M]_0/[CTA]_0/[I]_0$	Time (h)	Conv.[a] (%)	$M_{n,NMR}$[b] (g·mol^{-1})	$M_{n,SEC}$[c] (g·mol^{-1})	$Đ$
$PHPMA_{32}$-mCTA	100/1/0.2	3	91	4 130	4 335	1.21
$PHPMA_{32}$-*b*-$PDPA_{30}$	30/2/0.2	16	89	11 090	10 600	1.25
$PHPMA_{32}$-*b*-$PDPA_{97}$	97/2/0.2	16	84	25 360	25 610	1.28

[a]Determined by ^{1}H NMR spectroscopy in methanol-d_4 and acidic D_2O using end-group analysis;
[b]M_n was calculated *via* ^{1}H NMR spectroscopy according to $M_n = (n\text{MU} \times M_{W\ HPMA}) + (n\text{MU} \times M_{W\ monomer}) + M_{WCTA}$ eq. 1;
[c]Determined by SEC in methanol/acetate buffer, pH 6.5, 80/20 vol%.

2.6. Self-Assembly of spin labeled PHPMA-b-PDPA BCs in microfluidic Chips and characterization of RNPs

The self-assembled nanostructures were formed using a MF device purchased from Dolomite (Royston, United Kingdom). This MF device utilizes a sequential lamination micromixer chip, also known as a split-and-recombine (SAR) micromixer, which enhances mixing efficiency through exponential increase in contact surface area and reduction in path length. To initiate the self-assembly process, spin labeled PHPMA-*b*-PDPA BCs were dissolved in THF/methanol (80/20, v/v) and/or DMF at a concentration of 5.0 mg·mL^{-1}. The choice of solvents, a mixture of THF/methanol and/or DMF, as well as the used concentration was due to their excellent ability to dissolve the studied diblock copolymers. This is crucial for preventing the formation of macroscopic aggregates within the microfluidic chip. The polymer solution was pumped through the central channel, while PBS was introduced through the side channels using two independent Dolomite Mitos P-Pump systems (Royston, United Kingdom), controlled by computer software. Flow rates were adjustable parameters, and the resulting polymer colloids were collected in vials. Subsequently, the TEMPO-labeled PHPMA-*b*-PDPA nanoparticles (RNPs) were purified using a Sephadex G50 column in PBS (pH 7.4) to remove organic solvents and any residual unreacted TEMPO radicals. The supramolecular polymer assemblies were then characterized using dynamic light scattering (DLS), static light scattering (SLS), electrophoretic light scattering (ELS), transmission electron microscopy (TEM) and cryo-transmission electron microscopy (cryo-TEM).

3. Results and discussion

3.1. Synthesis of spin labeled $PHPMA_{32}$-b-$PDPA_n$ BCs

The strategic placement of the spin label within BCs is pivotal, offering insights into their self-assembly process. When positioned at the terminus of the hydrophilic block in self-assembling block copolymers, it facilitates the creation of detectable NPs with the label directly on the polymeric assemblies' surface. Following this principle, poly([*N*-(2-hydroxypropyl)]methacrylamide)-*b*-poly[2-(diisopropylamino)ethyl methacrylate] (PHPMA-*b*-PDPA) diblock copolymers were synthesized successfully *via* RAFT polymerization. Initially, well-defined PHPMA macroCTA was synthesized using RAFT polymerization (M_n = 4335 g/mol, M_w/M_n = 1.21). The polymerization followed a previously published protocol [42] using a MW reactor at 75 °C, employing 4-cyano-4-(((ethylthio)carbonothioyl)-thio)pentanoic acid as CTA and 4,4′-azobis (4-cyanovaleric acid) (V-501) as the initiator (Scheme 1, step1). Subsequently, the second block was grown from PHPMA-mCTA also *via* RAFT polymerization, depicted in Scheme 1, step 2. Finally, the DCC method was employed to covalently attach the 4-amino-2,2,6,6-tetramethylpiperidine-1-oxyl (TEMPO) end-group to the PHPMA block in the resulting PHPMA-*b*-PDPA BCs, generating stable TEMPO radicals (Scheme 1, step 3).

The chemical structure, composition, molecular weight, and dispersity index of PHPMA-mCTA and the resulting pH-responsive PHPMA-*b*-$PDPA_m$ BCs were confirmed using ^{1}H NMR spectroscopy (representative spectra for PHPMA-mCTA in Fig. S3 and PHPMA-*b*-PDPA in Fig. S4, as shown in the ESI) and size exclusion chromatography (SEC) (Fig. S5 in ESI).

The ^{1}H NMR spectrum of the PHPMA-mCTA RAFT agent was

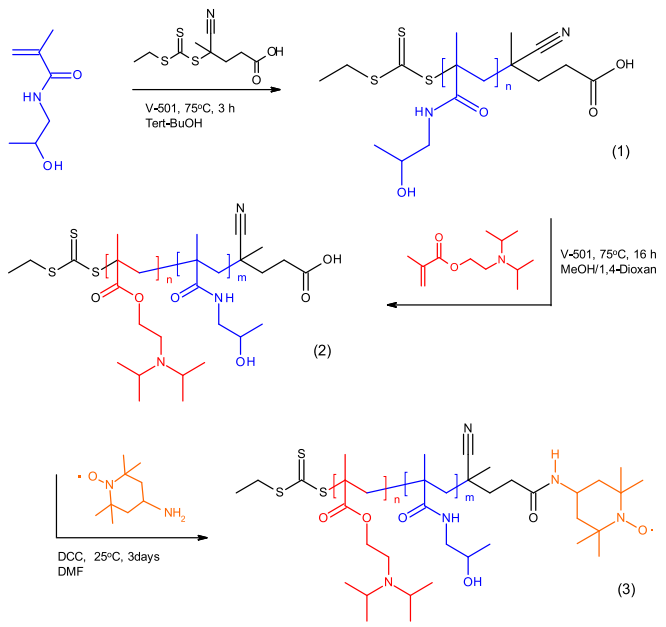

Scheme 1. The synthetic route for preparing PHPMA-*b*-PDPA block copolymers with incorporated TEMPO groups.

recorded, and the assignments of the different signals were made (see Fig. S3 in ESI). ^{1}H NMR revealed the complete disappearance of signals at $\delta = 5.68$ and 5.25 ppm, attributed to the vinyl protons from the HPMA monomer (marked as **b** in Fig. S1, ESI). A broad singlet was detected at 7.20–7.6 ppm ($-C(O)-NH-$) for the amide group in the composition of PHPMA. A singlet at 4.8 ppm corresponds to the protons of the $-OH$ group from the HPMA repeating units, though this peak overlaps with the residual methanol-d_4. The broad singlet at $\delta = 3.9$ ppm (**d**) is attributed to the methine proton from the $-CH-(OH)$ group. Signals at 1.7–1.9 (**a**) and 1.2 ppm (**b**) were attributed to the methylene protons of the PHPMA-mCTA main chain. Additionally, signals characteristic of methylene ($-C(O)-NH-CH_2-$) at $\delta = 2.9$–3.25 ppm (**c**) and those in the range $\delta = 0.8$–1.3 ppm (**e**), typical of methyl groups from the PHPMA backbone ($(CH_3)C-CH_2-$), were also observed.

The ^{1}H NMR spectrum of the PHPMA-*b*-PDPA diblock copolymer (Fig. S4 in ESI) displays characteristic signals corresponding to methylene protons from the pendant group ($-C(O)-NH-CH_2-$) at $\delta = 3.0$–3.3 ppm, marked as (**c**). Additionally, it shows signals for methylene protons from the main PHPMA backbone, observed in the range $\delta = 0.50$–1.20 ppm and at $\delta = 1.15$ ppm, labeled as (**b** + **e**), corresponding to the ($(CH_3)C-CH_2-$) backbone and methyl groups from the pendant group ($CH_3-CH(OH)$), respectively. Signals from the PDPA main chain are also detected at $\delta = 1.15$ ppm (**b**) and $\delta = 1.17$–2.0 ppm (**a**). Furthermore, signals corresponding to the isopropyl group attached to the amino group are observed at $\delta = 3.78$ ppm and 1.35 ppm (**h** and **i**). Broad signals characteristic of methylene protons from the PDPA pendant group ($-C(O)-CH_2-CH_2-N<$) are seen at $\delta = 4.3$–4.4 and 3.5 ppm, marked as (**f** and **g**).

The SEC chromatogram of PHPMA-mCTA obtained via MWI-assisted RAFT polymerization reveals a monomodal distribution, as evidenced by overlapping SEC traces (black curve in Fig. S5, ESI). Moreover, analysis indicates that SEC curves for PHPMA$_{32}$-*b*-PDPA$_m$ BCs containing stable nitroxide radicals are also monomodal and symmetric, reflecting a narrow molecular weight distribution (red and green chromatograms in Fig. S5, ESI). Importantly, SEC traces confirm the absence of duplicated products with higher M_n values, maintaining consistency across measurements. Key molecular characteristics of PHPMA-mCTA and pH-responsive BCs are summarized in Table 1, affirming the well-controlled and living nature of the polymerization process [42].

3.2. Self-Assembly of spin labeled PHPMA$_{32}$-*b*-PDPA$_n$ BCs in microfluidic Chips and characterization of RNPs

The structural characterization of the RNPs produced by MF nanoprecipitation involved a combination of EPR with scattering and imaging techniques, namely DLS, SLS, ELS, SAXS, TEM and cryo-TEM. The size distributions obtained by DLS, as well as the SLS data for the RNPs prepared using DMF and/or THF/methanol solvents, are depicted in Fig. 2. The results from the light scattering characterization are summarized in Table 2.

The DLS data demonstrate the presence of monodisperse populations of NPs for all BCs samples (Fig. 2A). The values of molecular weight ($M_{w\,(NPs)}$) and R_G were determined, respectively, from the intercepts and slopes of the scattering profiles from SLS data (Fig. 2B) and are presented in Table 2. The values of $M_{w(NPs)}$ were used to calculate the aggregation number ($N_{agg} = M_{w(NPs)}/M_{w(polymer\ by\ SEC)}$) and particles density (d_{NPs}), whereas the values of R_G were used to calculate the structure-sensitive parameters ($\rho = R_G/R_H$) which are related to the morphologies of the produced RNPs. The experimental data indicate that the size of the produced nano-objects is influenced by the overall molecular weight of the block copolymer, which is determined by the length of the hydrophobic block. The DLS/SLS data indicate that the overall dimensions of the RNPs increase with the length of the hydrophobic PDPA block (Fig. 2, Table 2). For the RNPs prepared in DMF, the diameter of the RNPs ($2R_H = D_H$) increases from 39 to 79.6 nm, the radius of gyration (R_G) from 23.5 to 66.5 nm, and the weight-average molecular weight ($M_{w(RNPs)}$) from 2.30 to 6.65 x 10^{-6} g/mol. For the RNPs prepared in THF/methanol, D_H increases from 84 to 94 nm, R_G from 58.0 to 70.1 nm, and $M_{w(RNPs)}$ from 9.12 to 11.05 x 10^{-6} g/mol (Table 2). The RNPs densities were found to be similar, except for the RNPs of PHPMA$_{23}$-*b*-PDPA$_{30}$ prepared in DMF, which resulted in the production of denser particles. The ρ values determined for the RNPs assemblies were higher than predicted for homogenous hard sphere (0.77) and are typical values found for spherical block copolymer micelles [21]. The observed ζ-potential values (Table 2) are consistent with those reported for other PDPA-*b*-PHPMA-based assemblies, falling within the range typically observed for nanoparticles with effective shielding and steric stabilization provided by the PHPMA shell, as demonstrated by our work and that of others [38,43].

Furthermore, SAXS measurements were utilized as a robust analytical technique to validate the presence of RNPs morphologies. The scattering curves obtained for RNPs are depicted in Fig. 3.

The resulting scattering patterns show an increase in the dimensions of the inner structure of particles (SAXS core radius, R) with the length of the hydrophobic PDPA block (Fig. 3, Table 2). Specifically, R increases from 13.1 to 23.5 nm and from 21.7 to 31.4 nm for RNPs prepared in DMF and THF/methanol, respectively. Additionally, the similar near q^{-4} dependence observed in the SAXS profiles indicates the formation of core–shell spherical RNPs following the self-assembly process for both BCs. Together, these data and the corresponding curve fittings validate the self-assembly of PHPMA-*b*-PDPA BCs into spherical RNPs. The presence of spherical core–shell-like structures in the samples prepared from PHPMA$_{32}$-*b*-PDPA$_{30}$ and PHPMA$_{32}$-*b*-PDPA$_{97}$ block copolymers was further confirmed by cryo-TEM, as suggested by the SAXS data profiles (see Fig. 4).

The cryo-TEM images clearly depict well-defined spherical micelles, showcasing particle diameters ranging from approximately 25 to 90 nm (refer to Fig. 4 and Fig. S6 in ESI). In Fig. 4A, the PHPMA$_{32}$-*b*-PDPA$_{30}$ RNPs obtained in DMF solvent show a micelle phase with particle sizes around 35–45 nm. Conversely, the cryo-TEM image of PHPMA$_{32}$-*b*-PDPA$_{30}$ RNPs prepared in a mixture of THF/methanol solvents reveals uniform and well-defined spherical micelles with slightly larger particle diameters of 40–50 nm (see Fig. 4B). For PHPMA$_{32}$-*b*-PDPA$_{97}$ BCs prepared in both DMF and THF/methanol (Fig. 4C and D), the cryo-TEM images display uniform and clearly defined spherical micelles assembled with particle sizes ranging from approximately 45 to 70 nm.

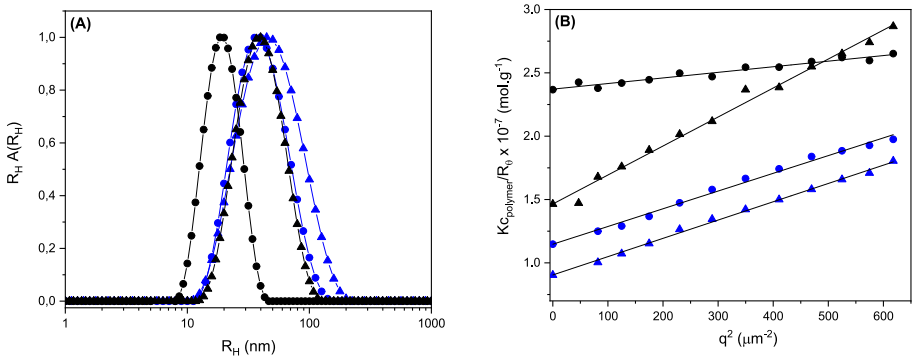

Fig. 2. Intensity-weighted size distributions (**A**) derived from REPES analysis of autocorrelation functions $C(q,t)$ observed at $\theta = 90°$, along with corresponding partial Zimm plots (**B**) for PHPMA$_{32}$-*b*-PDPA$_{30}$ (circles) and PHPMA$_{32}$-*b*-PDPA$_{97}$ (triangles) RNPs prepared in DMF (black) and THF/methanol (blue) (C_{final} = 5.0 mg mL^{-1}).

Table 2
Structural features of the fabricated block copolymer assemblies as determined by the scattering techniques.

Sample	Solvent	R_H (nm)	R_G (nm)	R_G/R_H	$M_{w\ (RNPs)} \times 10^6$ (g mol^{-1})	R (nm)[a]	N^b_{agg}	ζ (mV)[c]
PHPMA$_{32}$-*b*-PDPA$_{30}$	DMF	19.5	23.5	1.17	2.30	13.1	173	−4.9
	THF/MeOH	42.0	58.0	1.38	9.12	21.7	688	−4.6
PHPMA$_{32}$-*b*-PDPA$_{97}$	DMF	39.8	66.5	1.39	6.65	23.5	203	−5.1
	THF/MeOH	47.0	70.1	1.39	11.05	31.4	338	−5.8

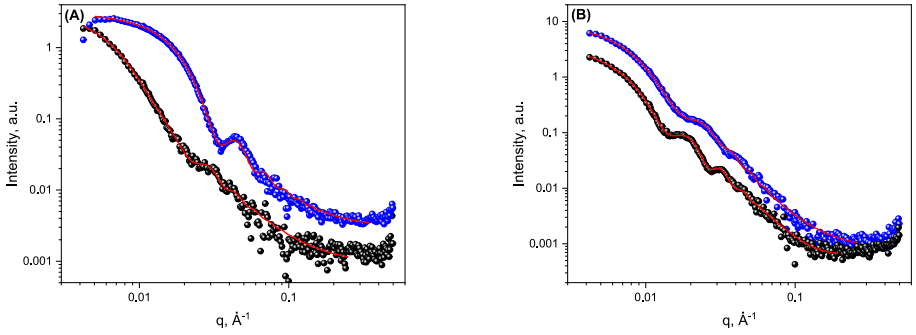

Fig. 3. SAXS patterns of (**A**) PHPMA$_{32}$-*b*-PDPA$_{30}$ and (**B**) PHPMA$_{32}$-*b*-PDPA$_{97}$ RNPs prepared using THF/methanol (black circles) and DMF (blue circles) accompanied by the corresponding curve fittings (red solid lines) (C_{final} = 5.0 mg mL^{-1}).

3.3. EPR Spectroscopic studies

The EPR spectra of TEMPO, PHPMA$_{32}$-*b*-PDPA$_{30}$ block copolymer and the NPs prepared by MF using different solvents are shown in Fig. 5. Nitroxide radicals exhibit characteristic triplet EPR spectra due to anisotropic hyperfine coupling between the unpaired electron and nitrogen nucleus.

Three narrow lines with almost equal intensities can be observed in the EPR spectrum of the unattached TEMPO radical in PBS solution, indicating very fast tumbling of the free nitroxide radical. After attachment of the nitroxide radical to the PHPMA$_{32}$-*b*-PDPA$_{30}$ copolymer the EPR signal becomes noticeably broader due to restricted radical mobility induced by covalent linkage at the end of PHPMA block. Two different components are observed in the EPR spectra of NPs prepared in DMF and THF/methanol. Fast component **F** represents the fraction of nitroxide radicals that originate from more mobile PHPMA, whereas the slow component **S** (marked with an arrow) represents the fraction with less mobile PHPMA. The two components were also observed previously in EPR spectra of NPs prepared from spin-labeled copolymers of poly(methylmethacrylate-*co*-acrylic acid) [44]. The mobility of the spin label was assessed by determining the rotational correlation time, τ_R, representing the time taken for the radical to rotate by one radian. To obtain these correlation times and analyze the slow and fast components, we simulated and compared EPR spectra recorded at 25 °C. Simulated EPR spectra of free TEMPO, PHPMA$_{32}$-*b*-PDPA$_{30}$ copolymer, and nanoparticles prepared in DMF and THF/methanol are depicted as dotted red lines in Fig. 5. The parameters used for simulating the EPR spectra are detailed in Table S1, and percentages of slow and fast components along with their corresponding rotational correlation times are presented in Table 3.

The very fast mobility of the free TEMPO radical with correlation time of only 0.03 ns is typical when the radical rotates in a medium of low local viscosity such as PBS solution. However, after covalent attachment of the radical to the PHPMA segment the τ_R value increased nine times when compared with free TEMPO (from 0.03 ns to 0.27 ns) indicating successful incorporation of the radical into the copolymer. The similar behavior was observed previously in spin labeled NPs based on PHPMA and cholesterol where the correlation time of the unattached radical in PBS solution increased from 0.03 ns to 0.20 ns upon attachment to the hydrophilic PHPMA copolymer [31]. After NPs preparation two different populations of radicals are observed, a fast population with τ_R values of 0.63 and 1.70 ns and slow population with τ_R values of 3.27 and 3.22 ns for NPs prepared in DMF and THF/methanol, respectively. These radicals can be assigned in two ways. A fast population represents

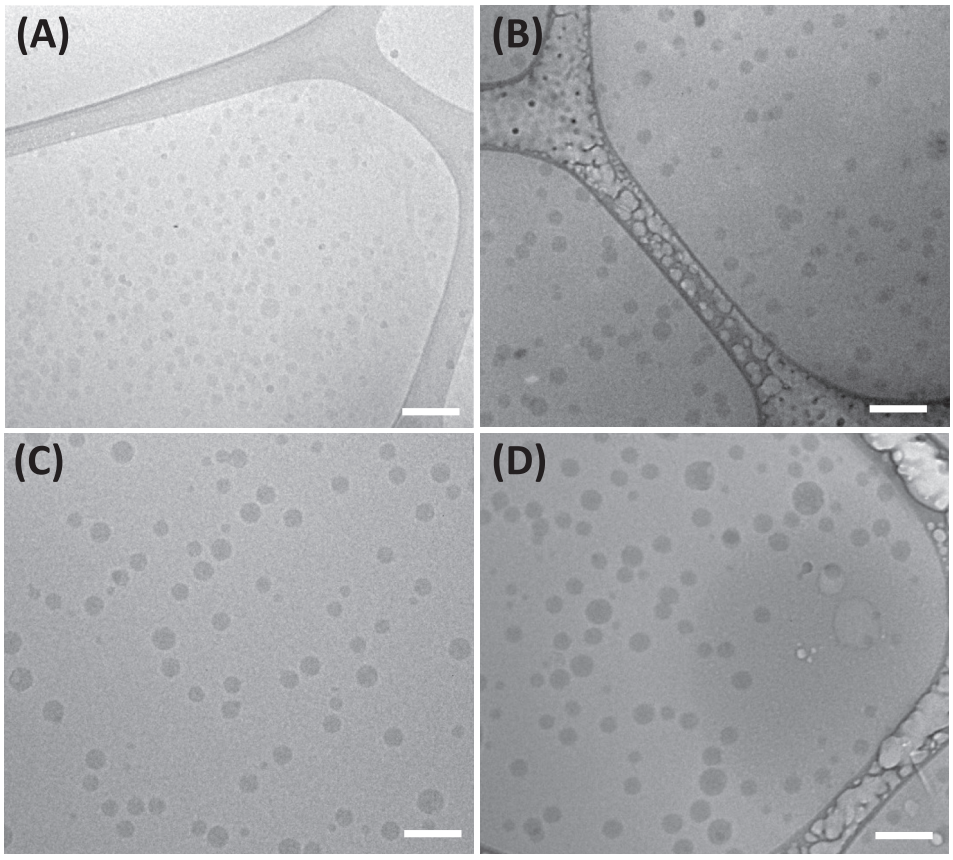

Fig. 4. Cryo-TEM images of self-assemblies of PHPMA$_{32}$-*b*-PDPA$_{30}$ prepared in DMF (**A**) and THF/methanol (**B**) and of PHPMA$_{32}$-*b*-PDPA$_{97}$ prepared in DMF (**C**) and THF/methanol (**D**). Scale bar = 100 nm.

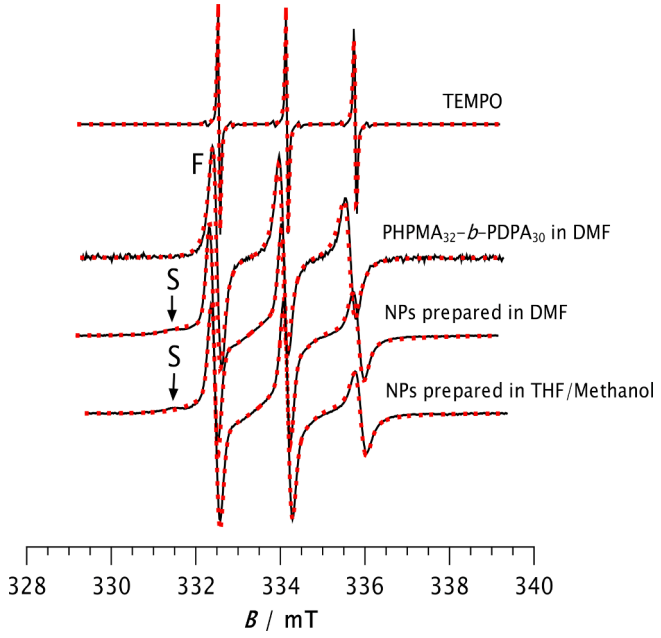

Fig. 5. EPR spectra of TEMPO in PBS, PHPMA$_{32}$-*b*-PDPA$_{30}$ block copolymer dissolved in DMF and of the nanoparticles prepared by MF using DMF and THF/methanol as organic solvents at 25 °C. Simulated spectra are shown as dotted red lines, while experimental spectra are shown as solid black lines.

Table 3
Percentages of slow and fast components and the calculated rotational correlation times for TEMPO, PHPMA$_{32}$-*b*-PDPA$_{30}$ copolymer and NPs prepared in DMF and THF/methanol measured at 25 °C.

Sample	Fast component		Slow component	
	Amount (%)	τ_R (ns)	Amount (%)	τ_R (ns)
TEMPO	100	0.03	–	–
PHPMA$_{32}$-*b*-PDPA$_{30}$	100	0.27	–	–
NPs prepared in DMF	42.8	0.63	57.2	3.27
NPs prepared in THF/methanol	39.6	1.70	60.4	3.22

the TEMPO radicals located on the PHPMA segment at the surface of the NPs, while the slow population represents the radicals bound to the part of the PHPMA segment that was captured within the core of NPs during preparation. Considering the cryo-TEM images and light-scattering data, PHPMA$_{32}$-*b*-PDPA$_{30}$ and PHPMA$_{32}$-*b*-PDPA$_{97}$ block copolymers are self-assembled to spherical micelles of various sizes. Taking into account the core–shell structure of the NPs, during microfluidic nanoprecipitation the particles grow by self-assembly of block copolymer from the random collision of primary nuclei (nucleation-aggregation) and the presence of hydrophilic blocks in the core of the NPs cannot be ruled out [45]. Therefore, it is expected that during the assembly process, a part of the PHPMA chains bearing TEMPO radical becomes trapped inside the core of the micelles [46] where the local density of the polymer increases, and the radical mobility becomes much more restricted with τ_R values of 3.27 ns and 3.22 ns for NPs prepared in DMF and THF/methanol, respectively (more than 100 times higher compared to the free TEMPO). On the other hand, the rotational mobility of the radicals located at the

surface of the NPs is only moderately slower compared to PHPMA$_{32}$-*b*-PDPA$_{30}$ copolymer. Moreover, the similar percentages of the slow and fast spectral components for NPs prepared in DMF and THF/methanol (57.2 % vs 60.4 % of slow component) indicate that the distribution of PHPMA chains bearing TEMPO radicals in NPs does not depend on the solvent used for the NPs preparation.

The nanoparticles self-assembled from PHPMA$_{32}$-*b*-PDPA$_{97}$ in DMF and THF/methanol show similar results and two components are again observed in ESR spectra, Fig. 6.

However, much larger τ_R values of 171.49 ns and 23.67 ns calculated for the slow component compared to nanoparticles assembled from PHPMA$_{32}$-*b*-PDPA$_{30}$ indicate that the mobility of radicals is very restricted because of higher polymer density originating from larger PDPA block, Tables 4 and S2. In addition, different percentages of slow and fast components for NPs prepared in DMF and THF/methanol (49.6 vs 78.5 % of slow component) indicate that the THF/methanol solvent mixture favors inclusion of the PHPMA block inside the nanoparticles. The observed differences in the mobility of radicals in particles prepared in DMF compared to those prepared in THF/methanol are attributed to the distinct assembly processes in these solvents.

Previous studies have shown that the thermodynamic solvent–water interaction parameter ($\chi_{solvent\text{-}water}$) significantly influences the nanoprecipitation step. The $\chi_{solvent\text{-}water}$ parameter describes the solvent–water affinity; lower $\chi_{solvent\text{-}water}$ values indicate higher solvent–water affinity, leading to the formation of smaller nanoparticles [47,48]. This trend aligns with our findings, as RNPs prepared in DMF, which has a lower $\chi_{solvent\text{-}water}$, are smaller than those prepared in THF/methanol, which has a higher $\chi_{solvent\text{-}water}$ value. The lower $\chi_{solvent\text{-}water}$ results in smaller and faster-forming nuclei during nanoprecipitation. This behavior affects not only particle size but also the internal particle structure, as observed by EPR. It is likely that primary nuclei formed during nanoprecipitation in THF/methanol are larger, more hydrophobic, and have a less stable interface, leading to random coalescence. In contrast, nuclei formed in DMF are smaller, less hydrophobic, and more stable. Consequently, RNPs prepared in THF/methanol are expected to trap a higher number of hydrophilic groups within their inner structure compared to those prepared in DMF.

Finally, the stimuli-responsive properties of the RNPs were evaluated under acidic conditions using EPR. The results are shown in Fig. 7 for PHPMA$_{32}$-*b*-PDPA$_{30}$ RNPs and in Fig. 8 for PHPMA$_{32}$-*b*-PDPA$_{97}$ RNPs.

As described previously, the EPR spectra of PHPMA$_{32}$-*b*-PDPA$_{30}$ block copolymer RNPs prepared using THF/methanol and DMF consist of slow and fast components because of different distribution of radicals in the core–shell spherical nanoparticles (see Fig. 7). After addition of HCl the slow component disappears and only one component remains in

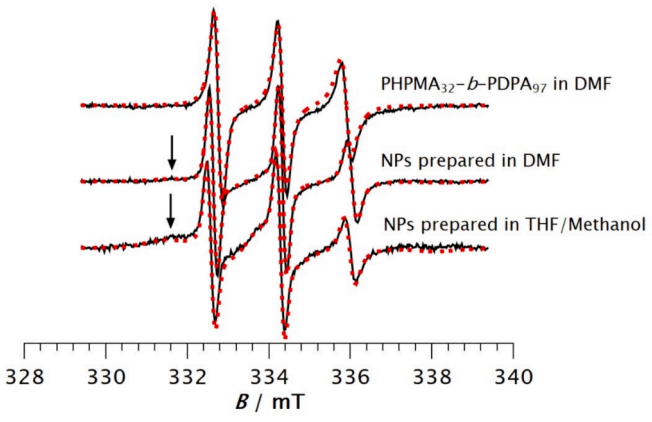

Fig. 6. EPR spectra of PHPMA$_{32}$-*b*-PDPA$_{97}$ block copolymer dissolved in DMF and of the NPs prepared by MF using DMF and THF/methanol as organic solvents at 25 °C. Simulated spectra are shown as dotted red lines, while experimental spectra are shown as solid black lines.

Table 4
Percentages of slow and fast components and the calculated rotational correlation times for free TEMPO, PHPMA$_{32}$-*b*-PDPA$_{97}$ copolymer and NPs prepared in DMF and THF/methanol measured at 25 °C.

Sample	Fast component		Slow component	
	Amount (%)	τ_R (ns)	Amount (%)	τ_R (ns)
TEMPO	100	0.03	–	–
PHPMA$_{32}$-*b*-PDPA$_{97}$	100	0.79	–	–
NPs prepared in DMF	50.4	0.50	49.6	171.49
NPs prepared in THF/methanol	21.5	0.56	78.5	23.67

the EPR spectra. The calculated τ_R values (Tables 5 and S3) reveal that the mobility of radicals after addition of the HCl for both NPs is comparable to the label in PHPMA$_{32}$-*b*-PDPA$_{30}$ copolymer before the self-assembly process. The addition of HCl clearly induces structural disassembly of the RNPs, as observed by TEM measurements (Fig. S7, ESI). Consequently, the radicals previously trapped inside the nanoparticles are exposed to the solution, allowing their mobility to be restored. The PHPMA$_{32}$-*b*-PDPA$_{97}$ block copolymer RNPs show comparable behavior (Fig. 8, Tables 6 and S4). After addition of HCl the structural disassembly of NPs is followed by the disappearance of the slow component from the EPR spectra. Again, the radicals that were significantly restricted in the dense regions inside the NPs are exposed to the solution and the correlation time for both NPs approaches the value obtained for spin labeled PHPMA$_{32}$-*b*-PDPA$_{97}$ block copolymer before micellization (0.79 ns) indicating complete disassembly of NPs.

Altogether, this study highlights the electron paramagnetic resonance spectroscopy as a valuable tool in the analysis of nanoparticles. EPR spectroscopy confirmed the successful formation of core–shell RNPs, with results closely matching the size and density measurements obtained from scattering techniques such as DLS, SLS, ELS SAXS, TEM and cryo-TEM. This investigation showcases the EPR-spin label approach's effectiveness in analyzing the internal structural characteristics and dynamics of core–shell nanoparticles and their response to pH-induced disassembly. For relevant data on the PDPA-*b*-PHPMA block as a drug delivery system, including encapsulation efficiency, drug delivery and release, and in vivo efficacy, readers should refer to our previous papers [38,39,49].

4. Conclusion

The pH-responsive PHPMA$_{32}$-*b*-PDPA$_n$ diblock copolymers, enriched with stable nitroxide radicals, were successfully synthesized using a combination of RAFT and DCC methods. This synthesis produced diblock copolymers with PDPA blocks of varying molecular weights, demonstrating precise control over the molecular characteristics of each product. The presence of TEMPO radicals was confirmed using EPR spectroscopy. Furthermore, employing the MF method, we primarily developed micellar structures, using pH-responsive amphiphilic TEMPO-PHPMA-*b*-PDPA copolymers. Additionally, EPR was utilized to investigate the dynamics within the prepared RNPs under buffer-simulated physiological conditions. Our findings revealed that the nitroxide radicals were distributed both within the core and on the surface of the NPs.

To assess their pH-responsiveness under buffer-simulated physiological conditions, both types of NPs underwent testing under acidic conditions typical of tumor sites. Upon the addition of hydrochloric acid, the nanoparticles underwent disassembly, confirming their pH-responsiveness.

These radical-containing nano-objects show promise for drug delivery applications, particularly in tumor patients where pH-responsiveness is crucial. Moreover, since RNPs are easily detectable using the EPR technique, they could serve as valuable tools for

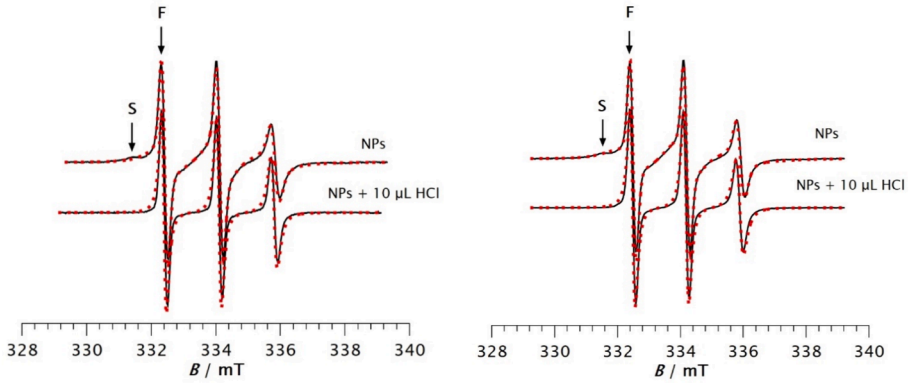

Fig. 7. EPR spectra of PHPMA$_{32}$-*b*-PDPA$_{30}$ block copolymer NPs prepared using THF/methanol (left) before and after addition of HCl and using DMF (right) before and after addition of HCl. Simulated spectra are shown as dotted red lines, while experimental spectra are shown as solid black lines.

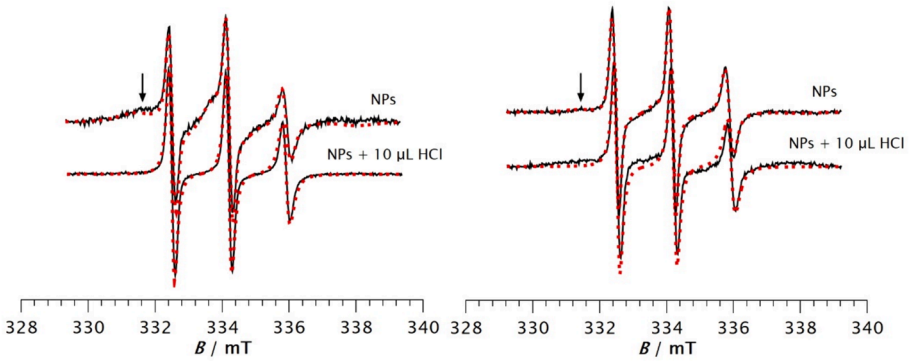

Fig. 8. EPR spectra of PHPMA$_{32}$-*b*-PDPA$_{97}$ block copolymer NPs prepared using THF/methanol (left) before and after addition of HCl and using DMF (right) before and after addition of HCl. Simulated spectra are shown as dotted red lines, while experimental spectra are shown as solid black lines.

Table 5
Percentages of slow and fast components and the calculated rotational correlation times for PHPMA$_{32}$-*b*-PDPA$_{30}$ block copolymer NPs prepared using THF/methanol before and after addition of HCl and using DMF before and after addition of HCl.

Sample	Fast component		Slow component	
	Amount (%)	τ_R (ns)	Amount (%)	τ_R (ns)
NPs prepared in THF/methanol	39.6	1.70	60.4	3.22
NPs prepared in THF/methanol + HCl	100	0.67	–	–
NPs prepared in DMF	42.8	0.63	57.2	3.27
NPs prepared in DMF + HCl	100	0.43	–	–

Table 6
Percentages of slow and fast components and the calculated rotational correlation times for PHPMA$_{32}$-*b*-PDPA$_{97}$ block copolymer NPs prepared using THF/methanol before and after addition of HCl and using DMF before and after addition of HCl.

Sample	**Fast component**		**Slow component**	
	Amount (%)	**τ_R (ns)**	**Amount (%)**	**τ_R (ns)**
NPs prepared in THF/methanol	21.5	0.56	78.5	23.67
NPs prepared in THF/methanol + HCl	100	1.42	–	–
NPs prepared in DMF	50.4	0.50	49.6	171.49
NPs prepared in DMF + HCl	100	0.85	–	–

monitoring drug pathways during patient treatment.

CRediT authorship contribution statement

Svetlana Lukáš Petrova: Writing – review & editing, Writing – original draft, Visualization, Formal analysis. **Alessandro Jäger:** Writing – original draft, Visualization, Methodology. **Ewa Pavlova:** Methodology. **Martina Vragović:** Methodology. **Eliézer Jäger:** Writing – review & editing, Supervision, Resources. **Miloš Steinhart:** Methodology, Formal analysis. **Damir Klepac:** Writing – review & editing, Writing – original draft, Methodology, Funding acquisition, Data curation.

Declaration of competing interest

The authors declare that they have no known competing financial interests or personal relationships that could have appeared to influence the work reported in this paper.

Data availability

Data will be made available on request.

Acknowledgments

The authors thank Miroslava Lukešová for conducting the EPR measurements of the spin labeled samples. This work has been partially supported by the University of Rijeka projects uniri-iskusni-prirod-23-207 and uniri-prirod-18-299. E.J. and A.J. acknowledges the sponsorship from the Ministry of Education, Youth and Sports of the Czech

Republic (grant # LUAUS24137).

Appendix A. Supplementary data

Supplementary data to this article can be found online at https://doi.org/10.1016/j.eurpolymj.2024.113473.

References

[1] S. Qiao, H. Wang, Temperature-responsive polymers: Synthesis, properties, and biomedical applications, Nano Res. 11 (2018) 5400–5423, https://doi.org/10.1007/s12274-018-2121-x.

[2] S. Lukáš Petrova, M. Vragović, E. Pavlova, Z. Černochová, A. Jäger, E. Jäger, R. Konefał, Smart poly(lactide)-b-poly(triethylene glycol methyl ether methacrylate) (PLA-b-PTEGMA) block copolymers: one-pot synthesis, temperature behavior, and controlled release of paclitaxel, Pharmaceutics 15 (2023) 1191, https://doi.org/10.3390/pharmaceutics15041191.

[3] J. Thévenot, H. Oliveira, O. Sandre, S. Lecommandoux, Magnetic responsive polymer composite materials, Chem. Soc. Rev. 42 (2013) 7099, https://doi.org/10.1039/c3cs60058k.

[4] M. Wei, Y. Gao, X. Li, M.J. Serpe, Stimuli-responsive polymers and their applications, Polym. Chem. 8 (2016) 127–143, https://doi.org/10.1039/C6PY01585A.

[5] A. Bratek-Skicki, Towards a new class of stimuli-responsive polymer-based materials – Recent advances and challenges, Applied Surface Science Advances 4 (2021) 100068, https://doi.org/10.1016/j.apsadv.2021.100068.

[6] Y. Shymborska, A. Budkowski, J. Raczkowska, V. Donchak, Y. Melnyk, V. Vasiichuk, Y. Stetsyshyn, Switching it Up: The Promise of Stimuli-Responsive Polymer Systems in Biomedical Science, Chem. Rec. 24 (2024) e202300217.

[7] S. Mura, J. Nicolas, P. Couvreur, Stimuli-responsive nanocarriers for drug delivery, Nature Mater 12 (2013) 991–1003, https://doi.org/10.1038/nmat3776.

[8] B. Nandan, A. Horechyy, Hairy core-shell polymer nano-objects from self-assembled block copolymer structures, ACS Appl. Mater. Interfaces 7 (2015) 12539–12558, https://doi.org/10.1021/am5075503.

[9] Y. Liu, G. Yang, Y. Hui, S. Ranaweera, C.-X. Zhao, Microfluidic nanoparticles for drug delivery, Small 18 (2022) 2106580, https://doi.org/10.1002/smll.202106580.

[10] J.P. Martins, G. Torrieri, H.A. Santos, The importance of microfluidics for the preparation of nanoparticles as advanced drug delivery systems, Expert Opin. Drug Deliv. 15 (2018) 469–479, https://doi.org/10.1080/17425247.2018.1446936.

[11] J. Xu, S. Zhang, A. Machado, S. Lecommandoux, O. Sandre, F. Gu, A. Colin, Controllable microfluidic production of drug-loaded plga nanoparticles using partially water-miscible mixed solvent microdroplets as a precursor, Sci Rep 7 (2017) 4794, https://doi.org/10.1038/s41598-017-05184-5.

[12] D. Liu, H. Zhang, B. Herranz-Blanco, E. Mäkilä, V. Lehto, J. Salonen, J. Hirvonen, H.A. Santos, Microfluidic assembly of monodisperse multistage ph-responsive polymer/porous silicon composites for precisely controlled multi-drug delivery, Small 10 (2014) 2029–2038, https://doi.org/10.1002/smll.201303740.

[13] X. Zhang, G. Chen, L. Liu, L. Zhu, Z. Tong, Precise control of two-dimensional platelet micelles from biodegradable poly(p-dioxanone) block copolymers by crystallization-driven self-assembly, Macromolecules 55 (2022) 8250–8261, https://doi.org/10.1021/acs.macromol.2c01158.

[14] Z. Tong, Y. Xie, M.C. Arno, Y. Zhang, I. Manners, R.K. O'Reilly, A.P. Dove, Uniform segmented platelet micelles with compositionally distinct and selectively degradable cores, Nat. Chem. 15 (2023) 824–831, https://doi.org/10.1038/s41557-023-01177-2.

[15] L. Liu, C.T.J. Ferguson, L. Zhu, S. Chen, R.-Y. Wang, S. Wang, A.P. Dove, R. K. O'Reilly, Z. Tong, Synthesis of hollow platelet polymer particles by spontaneous precision fragmentation, Nat. Synth 3 (2024) 903–912, https://doi.org/10.1038/s44160-024-00554-0.

[16] X. Zhang, G. Chen, B. Zheng, Z. Wan, L. Liu, L. Zhu, Y. Xie, Z. Tong, Uniform Two-Dimensional Crystalline Platelets with Tailored Compositions for pH Stimulus-Responsive Drug Release, Biomacromolecules 24 (2023) 1032–1041, https://doi.org/10.1021/acs.biomac.2c01481.

[17] P. Černoch, A. Jager, Z. Černochová, V. Sincari, L.J.C. Albuquerque, R. Konefal, E. Pavlova, F.C. Giacomelli, E. Jager, Engineering of pH-triggered nanoplatforms based on novel poly(2-methyl-2-oxazoline)- *b* -poly[2-(diisopropylamino)ethyl methacrylate] diblock copolymers with tunable morphologies for biomedical applications, Polym. Chem. 12 (2021) 2868–2880, https://doi.org/10.1039/D1PY00141H.

[18] H. Lomas, J. Du, I. Canton, J. Madsen, N. Warren, S.P. Armes, A.L. Lewis, G. Battaglia, Efficient encapsulation of plasmid DNA in pH-sensitive PMPC–PDPA polymersomes: study of the effect of PDPA block length on copolymer–DNA binding affinity, Macromol. Biosci. 10 (2010) 513–530, https://doi.org/10.1002/mabi.201000083.

[19] H. Lomas, I. Canton, S. MacNeil, J. Du, S.P. Armes, A.J. Ryan, A.L. Lewis, G. Battaglia, Biomimetic pH sensitive polymersomes for efficient DNA encapsulation and delivery, Adv. Mater. 19 (2007) 4238–4243, https://doi.org/10.1002/adma.200700941.

[20] I. Canton, G. Battaglia, Endocytosis at the nanoscale, Chem. Soc. Rev. 41 (2012) 2718, https://doi.org/10.1039/c2cs15309b.

[21] F.C. Giacomelli, P. Stepánek, C. Giacomelli, V. Schmidt, E. Jäger, A. Jäger, K. Ulbrich, pH-triggered block copolymer micelles based on a pH-responsive PDPA (poly[2-(diisopropylamino)ethyl methacrylate]) inner core and a PEO (poly (ethylene oxide)) outer shell as a potential tool for the cancer therapy, Soft Matter 7 (2011) 9316, https://doi.org/10.1039/c1sm05992k.

[22] C. Pegoraro, D. Cecchin, L.S. Gracia, N. Warren, J. Madsen, S.P. Armes, A. Lewis, S. MacNeil, G. Battaglia, Enhanced drug delivery to melanoma cells using PMPC-PDPA polymersomes, Cancer Lett. 334 (2013) 328–337, https://doi.org/10.1016/j.canlet.2013.02.007.

[23] J.A. Alfurhood, H. Sun, P.R. Bachler, B.S. Sumerlin, Hyperbranched poly(N-(2-hydroxypropyl) methacrylamide) via RAFT self-condensing vinyl polymerization, Polym. Chem. 7 (2016) 2099–2104, https://doi.org/10.1039/C6PY00111D.

[24] E. Randárová, H. Nakamura, R. Islam, M. Studenovský, H. Mamoru, J. Fang, P. Chytil, T. Etrych, Highly effective anti-tumor nanomedicines based on HPMA copolymer conjugates with pirarubicin prepared by controlled RAFT polymerization, Acta Biomater. 106 (2020) 256–266, https://doi.org/10.1016/j.actbio.2020.02.011.

[25] X. Zhang, B.-J. Niebuur, P. Chytil, T. Etrych, S.K. Filippov, A. Kikhney, D.C. F. Wieland, D.I. Svergun, C.M. Papadakis, Macromolecular pHPMA-based nanoparticles with cholesterol for solid tumor targeting: behavior in HSA protein environment, Biomacromolecules 19 (2018) 470–480, https://doi.org/10.1021/acs.biomac.7b01579.

[26] Y. Bobde, S. Biswas, B. Ghosh, Current trends in the development of HPMA-based block copolymeric nanoparticles for their application in drug delivery, Eur. Polym. J. 139 (2020) 110018, https://doi.org/10.1016/j.eurpolymj.2020.110018.

[27] T.T. Hoang Thi, E.H. Pilkington, D.H. Nguyen, J.S. Lee, K.D. Park, N.P. Truong, The importance of poly(ethylene glycol) alternatives for overcoming PEG immunogenicity in drug delivery and bioconjugation, Polymers 12 (2020) 298, https://doi.org/10.3390/polym12020298.

[28] S. Petrova, D. Klepac, R. Konefał, S. Kereïche, L. Kováčik, S.K. Filippov, Synthesis and solution properties of PCL-b-PHPMA diblock copolymers containing stable nitroxyl radicals, Macromolecules 49 (2016) 5407–5417, https://doi.org/10.1021/acs.macromol.6b01187.

[29] S. Valić, M. Andreis, D. Klepac, ESR Spectroscopy of Multiphase Polymer Systems, in: A. Boudenne, L. Ibos, Y. Candau, S. Thomas (Eds.), Handbook of Multiphase Polymer Systems, 1st ed.,, Wiley, 2011, pp. 551–584, https://doi.org/10.1002/9781119972020.ch14.

[30] Y. Li, M.S. Budamagunta, J. Luo, W. Xiao, J.C. Voss, K.S. Lam, Probing of the assembly structure and dynamics within nanoparticles during interaction with blood proteins, ACS Nano 6 (2012) 9485–9495, https://doi.org/10.1021/nn302317j.

[31] D. Klepac, H. Kostková, S. Petrova, P. Chytil, T. Etrych, S. Kereïche, I. Raška, D. A. Weitz, S.K. Filippov, Interaction of spin-labeled HPMA-based nanoparticles with human blood plasma proteins – the introduction of protein-corona-free polymer nanomedicine, Nanoscale 10 (2018) 6194–6204, https://doi.org/10.1039/C7NR09355A.

[32] T. Yoshitomi, K. Kuramochi, L. Binh Vong, Y. Nagasaki, Development of nitroxide radicals–containing polymer for scavenging reactive oxygen species from cigarette smoke, Sci. Technol. Adv. Mater. 15 (2014) 035002, https://doi.org/10.1088/1468-6996/15/3/035002.

[33] T. Yoshitomi, Y. Nagasaki, Nitroxyl radical-containing nanoparticles for novel nanomedicine against oxidative stress injury, Nanomedicine 6 (2011) 509–518, https://doi.org/10.2217/nnm.11.13.

[34] B. Shashni, Y. Nagasaki, Nitroxide radical-containing nanoparticles attenuate tumorigenic potential of triple negative breast cancer, Biomaterials 178 (2018) 48–62, https://doi.org/10.1016/j.biomaterials.2018.05.042.

[35] B. Shashni, Y. Nishikawa, Y. Nagasaki, Management of tumor growth and angiogenesis in triple-negative breast cancer by using redox nanoparticles, Biomaterials 269 (2021) 120645, https://doi.org/10.1016/j.biomaterials.2020.120645.

[36] L.B. Vong, T. Yoshitomi, H. Matsui, Y. Nagasaki, Development of an oral nanotherapeutics using redox nanoparticles for treatment of colitis-associated colon cancer, Biomaterials 55 (2015) 54–63, https://doi.org/10.1016/j.biomaterials.2015.03.037.

[37] L.J.C. Albuquerque, V. Sincari, A. Jäger, R. Konefał, J. Pánek, P. Černoch, E. Pavlova, P. Štěpánek, F.C. Giacomelli, E. Jäger, Microfluidic-assisted engineering of quasi-monodisperse ph-responsive polymersomes toward advanced platforms for the intracellular delivery of hydrophilic therapeutics, acs.langmuir.9b01009, Langmuir (2019), https://doi.org/10.1021/acs.langmuir.9b01009.

[38] L.J.C. Albuquerque, V. Sincari, A. Jäger, J. Kucka, J. Humajova, J. Pankrac, P. Paral, T. Heizer, O. Janouškova, I. Davidovich, Y. Talmon, P. Pouckova, P. Štěpánek, L. Sefc, M. Hruby, F.C. Giacomelli, E. Jäger, pH-responsive polymersome-mediated delivery of doxorubicin into tumor sites enhances the therapeutic efficacy and reduces cardiotoxic effects, J. Control. Release 332 (2021) 529–538, https://doi.org/10.1016/j.jconrel.2021.03.013.

[39] E. Jäger, P. Černoch, M. Vragovic, L.J. Calumby Albuquerque, V. Sincari, T. Heizer, A. Jäger, J. Kučka, O.Š. Janoušková, E. Pavlova, L. Šefc, F.C. Giacomelli, Membrane permeability and responsiveness drive performance: linking structural features with the antitumor effectiveness of doxorubicin-loaded stimuli-triggered polymersomes, Biomacromolecules 25 (2024) 4192–4202, https://doi.org/10.1021/acs.biomac.4c00282.

[40] K. Ulbrich, V. Šubr, J. Strohalm, D. Plocová, M. Jelínková, B. Říhová, Polymeric drugs based on conjugates of synthetic and natural macromolecules, J. Control. Release 64 (2000) 63–79, https://doi.org/10.1016/S0168-3659(99)00141-8.

[41] M. Danial, S. Telwatte, D. Tyssen, S. Cosson, G. Tachedjian, G. Moad, A. Postma, Combination anti-HIV therapy via tandem release of prodrugs from

macromolecular carriers, Polym. Chem. 7 (2016) 7477–7487, https://doi.org/10.1039/C6PY01882C.
[42] V. Sincari, S.L. Petrova, R. Konefał, M. Hruby, E. Jäger, Microwave-assisted RAFT polymerization of N-(2-hydroxypropyl) methacrylamide and its relevant copolymers, React. Funct. Polym. 162 (2021) 104875, https://doi.org/10.1016/j.reactfunctpolym.2021.104875.
[43] I. Alberg, S. Kramer, M. Schinnerer, Q. Hu, C. Seidl, C. Leps, N. Drude, D. Möckel, C. Rijcken, T. Lammers, M. Diken, M. Maskos, S. Morsbach, K. Landfester, S. Tenzer, M. Barz, R. Zentel, Polymeric Nanoparticles with Neglectable Protein Corona, Small 16 (2020) 1907574, https://doi.org/10.1002/smll.201907574.
[44] M.A. Uddin, H. Yu, L. Wang, K.-R. Naveed, B.U. Amin, S. Mehmood, F. Haq, A. Nazir, T. Lin, X. Chen, Z. Ni, Multiple-stimuli-responsiveness and conformational inversion of smart supramolecular nanoparticles assembled from spin labeled amphiphilic random copolymers, J. Colloid Interface Sci. 585 (2021) 237–249, https://doi.org/10.1016/j.jcis.2020.11.042.
[45] R. Karnik, F. Gu, P. Basto, C. Cannizzaro, L. Dean, W. Kyei-Manu, R. Langer, O. C. Farokhzad, Microfluidic Platform for Controlled Synthesis of Polymeric Nanoparticles, Nano Lett. 8 (2008) 2906–2912, https://doi.org/10.1021/nl801736q.
[46] J. Grundler, K. Shin, H.-W. Suh, M. Zhong, W.M. Saltzman, Surface topography of polyethylene glycol shell nanoparticles formed from bottlebrush block copolymers controls interactions with proteins and cells, ACS Nano 15 (2021) 16118–16129, https://doi.org/10.1021/acsnano.1c04835.
[47] A.M. De Oliveira, E. Jäger, A. Jäger, P. Stepánek, F.C. Giacomelli, Physicochemical aspects behind the size of biodegradable polymeric nanoparticles: A step forward, Colloids Surf. A Physicochem. Eng. Asp 436 (2013) 1092–1102, https://doi.org/10.1016/j.colsurfa.2013.08.056.
[48] M. Beck-Broichsitter, J. Nicolas, P. Couvreur, Solvent selection causes remarkable shifts of the “Ouzo region” for poly(lactide-co-glycolide) nanoparticles prepared by nanoprecipitation, Nanoscale 7 (2015) 9215–9221, https://doi.org/10.1039/C5NR01695A.
[49] E. Jäger, V. Sincari, L.J.C. Albuquerque, A. Jäger, J. Humajova, J. Kucka, J. Pankrac, P. Paral, T. Heizer, O. Janouskova, R. Konefał, E. Pavlova, O. Sedlacek, F.C. Giacomelli, P. Pouckova, L. Sefc, P. Stepanek, M. Hruby, Reactive oxygen species (ROS)-responsive polymersomes with site-specific chemotherapeutic delivery into tumors via spacer design Chemistry, Biomacromolecules 21 (2020) 1437–1449, https://doi.org/10.1021/acs.biomac.9b01748.